Molecular BioSystems

Cite this: *Mol. BioSyst.*, 2011, **7**, 1409–1419

www.rsc.org/molecularbiosystems

PAPER

Tracking cellular metabolomics in lipoapoptosis- and steatosis-developing liver cells

Yasushi Noguchi, Jamey D. Young, Jose O. Aleman, Michael E. Hansen, Joanne K. Kelleher and Gregory Stephanopoulos*

Received 2nd December 2010, Accepted 24th January 2011
DOI: 10.1039/c0mb00309c

Palmitate (PA) is known to induce reactive oxygen species (ROS) formation and apoptosis in liver cells, whereas concurrent treatment of oleate (OA) with PA predominately induces steatosis without ROS in liver cells. We previously reported that PA treatment induces the decoupling of glycolysis and tricarboxylic acid cycle (TCA cycle) fluxes, but OA co-treatment restored most metabolic fluxes to their control levels. However, the mechanisms by which metabolites are linked to metabolic fluxes and subsequent lipoapoptotic or steatotic phenotypes remain unclear. To determine the link, we used GC-MS-based polar and non-polar metabolic profiling in lipoapoptosis- or steatosis-developing H4IIEC3 hepatoma cells, to examine the metabolome at different time points after treatment with either PA alone (PA cells) or both PA and OA (PA/OA cells). Metabolic profiles revealed various changes in metabolite levels for TCA cycle intermediates, pentose phosphate pathway (PPP) intermediates, and energy storage metabolites between PA and PA/OA cells. For example, adenosine was markedly increased only in PA cells, whereas gluconate was increased in PA/OA cells. To assess the interaction among these metabolites, the metabolite-to-metabolite correlations were calculated and correlation networks were visualized. These correlation networks demonstrate that a dissociation among PPP metabolites was introduced in PA-treated cells, and this dissociation was restored in PA/OA-treated cells. Thus, our data suggest that abnormal PPP fluxes, in addition to increased adenosine levels, might be related to the decoupling of glycolysis and the resulting lipoapoptotic phenotype.

Introduction

Analysis of the cellular metabolome is important when relating metabolites to cellular phenotype.[1,2] Various metabolomic studies have been reported in cellular models of drug response,[3] adipocytes,[4] viral infection,[5] carcinogenesis[6,7] and more recently embryonic stem cell differentiation.[8]

Elevated serum free fatty acids (FFA) cause hepatic apoptosis,[9] which is a prominent feature of non-alcoholic steatohepatitis (NASH) that correlates with disease severity.[10] Previous *in vitro* studies in Chinese hamster ovary (CHO) cells,[9,11] cardiac myocytes,[12] pancreatic β-cells,[13] and hepatic cells[14,15] demonstrated that saturated fatty acids (SFA), but not mono-unsaturated fatty acids (MUFAs), induce reactive oxygen species (ROS) generation and apoptosis, whereas MUFAs predominately induce steatosis. An earlier study showed that MUFA co-treatment changed the palmitate (PA)-induced phenotype from apoptosis to steatosis by diverting SFA into triglyceride synthesis, thereby reducing apoptosis in CHO cells.[11] Ceramide accumulation has been considered as a primary factor responsible for SFA-induced ROS generation and apoptosis because ceramides are synthesized *de novo* from PA and serine, and they also have been shown to activate apoptotic signaling.[16] More recent studies including ours, however, have reported that SFA can induce apoptosis through ROS formation[17] and endoplasmic reticulum stress, independent of intracellular ceramide levels.[18]

We previously examined metabolic flux using isotopic tracers to quantify phenotypic changes in H4IIEC3 hepatoma cells treated with either PA alone (PA cells) or a combination of PA and oleate (OA) (PA/OA cells).[17] Our results indicate that the FFA-induced ROS generation and apoptosis are accompanied by the decoupling of glycolytic and TCA cycle fluxes, leading to abnormal cytosolic redox states. However, the mechanism by which glycolytic and TCA cycle fluxes are disconnected by elevated serum FFA is still indistinct.

To further address this question, we hypothesized that there could be as yet unknown metabolites that contribute to the dissociation between glycolysis and the TCA cycle leading to ROS generation in the early phases of apoptosis in cells. In the current study, we conducted GC-MS-based comprehensive profiling of polar and non-polar metabolites

Department of Chemical Engineering, Massachusetts Institute of Technology, Cambridge MA 02139, USA. E-mail: gregstep@mit.edu; Fax: +1 617-253-3122; Tel: +1 617-258-0398

to find metabolites corresponding to fatty acid induced apoptosis or steatosis in H4IIEC3 hepatoma cells. These metabolites were then correlated with other metabolites discovered separately in apoptotic and steatotic cells, to identify factors causing SFA-induced apoptosis and restoration of normal cellular metabolism by MUFA.

Results

PA-induced lipoapoptosis and restoration of normal cellular metabolism by OA under normal physiological amino acid concentrations

Previously, we showed that PA induced the decoupling of the glycolytic and TCA cycle fluxes in H4IIEC3 rat hepatoma cells cultured in media containing physiological amino acid concentrations, whereas treatment with OA in addition to PA restored most fluxes to normal levels.[17] Table 2 shows the influence of treatment with 400 μM PA or OA alone or co-treatment with 10, 50 or 200 μM OA on ROS concentration, cell viability and cellular lipid levels using growth medium containing the same amino acid composition. The data clearly show that the induction of ROS and cell death were caused by treatment with PA alone, whereas treatment with OA alone and concurrent treatment with OA and PA increased cellular lipid concentration (Table 2 and Fig. 1). Co-treatment with OA concentrations over 50 μM was sufficient to normalize PA-induced ROS generation and to restore cell viability (Fig. 1).

Treatment with PA disturbs cellular metabolite levels

In the present study, we investigated time-dependent changes in cellular metabolite concentrations after the treatment of H4IIEC3 cells with 400 μM PA alone (PA cells) or both 400 μM PA and 50 μM OA (PA/OA cells), to identify metabolites related to apoptosis and steatosis. We applied GC-MS based comprehensive metabolite profiling to untreated cells, PA-cells and PA/OA-cells after varying incubation times (3, 6 and 12 h). In these experiments, the amino acid concentrations were set at physiological levels (total amino acids = 2.15 mM). Representative GC-MS chromatograms of polar and non-polar metabolites from H4IIEC3 cells are shown in Fig. 3. Using our method, we were able to simultaneously observe concentrations of various amino acids, organic acids, nucleic acids and sugar metabolites from polar extracts in addition to concentrations of FFA, cholesterols, ceramides, monoacylglycerols and diacylglycerols from non-polar extracts (Fig. 2A and B). We identified a total of 468 peaks from polar (325 peaks) and non-polar (143 peaks) fractions obtained from H4IIEC3 cell lysates (data not shown). After the removal of non-reproducible peaks, we were left with a total of 254 well-conserved peaks and identified 107 metabolites from these peaks, using the NIST05 and in-house standard libraries as described in Experimental Procedures.

Fig. 3A shows the relative abundance (R.A.) of 254 metabolites against *p*-values derived from a 2-way ANOVA. The 33 most abundant and significant metabolites (R.A. $>$ 0.5 and $p < 0.00005$) from Fig. 3A were subjected to FDA to obtain a clear time-dependent separation among untreated cells, PA cells and PA/OA cells (Fig. 3B and C). In Fig. 3B and C, the $y1$ axis roughly corresponds to the steatotic phenotype, and the $y2$ axis represents the apoptotic phenotype. We identified marker metabolites including adenosine, malate, serine, citrate, aspartate, C16 ceramide and diacylglycerol (DAG) in PA cells and fructose, gluconate, glutamate and desmosterol in PA/OA cells. In addition, we found relatively high glycerate levels in both untreated and PA cells in comparison to PA/OA cells. A detailed list of these marker metabolites is presented in Table 3. We also explored low-abundance metabolites as phenotypic markers, as described in Fig. 4A (total 117 metabolites, R.A. $>$ 0.001 and $p < 0.00005$). Pearson (r) correlation analysis between the most and least abundant metabolites listed in Table 3 allowed the identification of pyruvate, galactonate and other minor ceramide species as additional markers (Fig. 3D). Representative correlation plots are shown in Fig. 4A. Pyruvate exhibited a clear positive correlation with adenosine. Serine, a marker of PA cells, showed a positive correlation with alanine but a negative correlation with gluconate, a marker of PA/OA cells (Fig. 4A). Time-dependent changes in phenotypic metabolites are shown in Fig. 4B. Cellular adenosine and pyruvate were strongly increased in PA cells from 3 to 6 h but were decreased at 12 h (Fig. 4B). Additionally, ceramide and 1,2 dipalmitoylglycerol (DAG) levels were continuously higher in PA cells than in PA/OA-cells (Fig. 4B). Both gluconate and galactonate were increased only in PA/OA cells (Fig. 4B). Glycerate, a product of glycerolipids, was consistently lower in PA/OA cells (Fig. 4B).

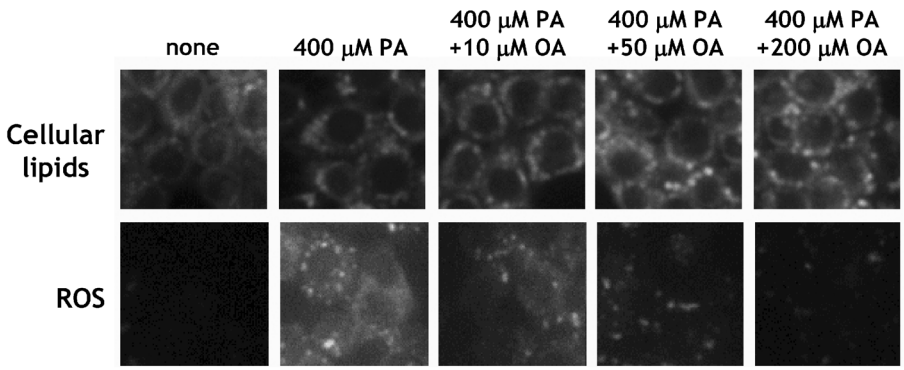

Fig. 1 Microscopic observations of FFA-induced lipid accumulation and ROS generation in H4IIEC3 cells. Cells were incubated with 400 μM palmitate (PA), 400 μM oleate (OA), 400 μM PA plus 10 μM or 50 μM OA or without FFA (none) for either 12 h (for ROS detection) or 24 h (for lipid detection). Cellular lipids and ROS were determined using Nile red and DCF fluorescence, respectively.

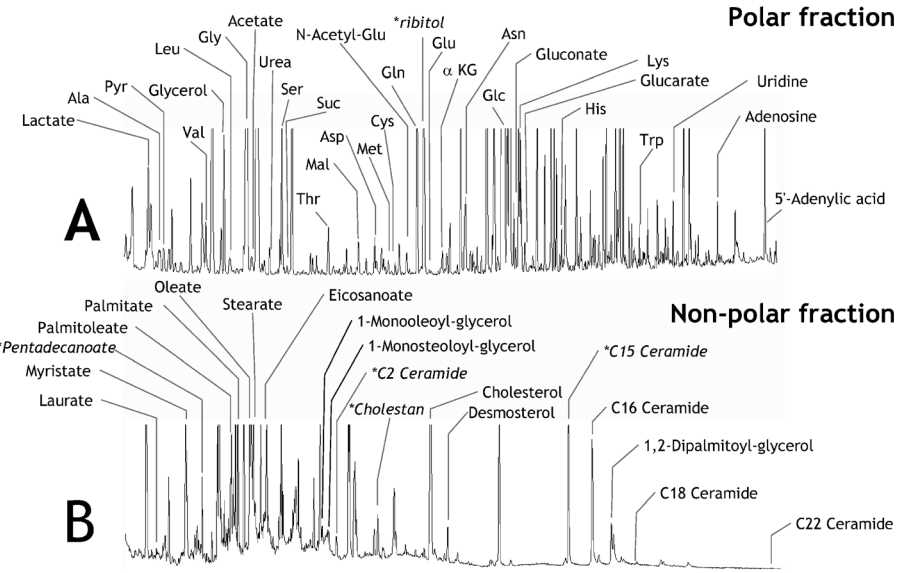

Fig. 2 Representative gas chromatography profiles of polar and non-polar metabolites from H4IIEC3 cells. A biphasic metabolite extraction was examined from H4IIEC3 cells grown in 100 mm dishes, with polar metabolites partitioning into a methanol/water phase (A) and non-polar metabolites partitioning into a chloroform phase (B). GC-MS analysis was performed as described in the Experimental Procedures with the non-polar internal standards 4.96 nmol pentadecanoate, 2.94 nmol 5α-cholestane and 4.2 nmol *N*-pentadecanoyl-sphingosine (C15 ceramide) in addition to the polar internal standards 9.9 nmol ribitol (shown in *italics*).

Comparison of metabolite–metabolite correlation between apoptotic and steatotic cells

Changes in metabolite–metabolite correlation pairs between control and apoptotic or steatotic phenotypes were assessed using a total of 117 metabolites (R.A. $>$ 0.001 and $p <$ 0.00005). We choose to use Spearman ρ for comparison of metabolite–metabolite correlated pairs because we found non-linear relationships in most of the scatter plots (Fig. 5A). Fig. 5A shows a histogram of the Spearman ρ between each metabolite-to-metabolite pair, where 6786 metabolite-to-metabolite pairs were generated from 117 metabolites. To examine whether FFA treatments altered the correlation between metabolite-to-metabolite pairs, the metabolite-to-metabolite pairs were arranged in order of the change in ρ between the two groups from the negative to positive maximum, leading to the finding that some of the metabolites were clearly sensitive to FFA treatment (Fig. 5B).

To assess the significance of correlated pairs, we determined a false discovery rate (FDR) by estimating a q-value for each correlated pair. Predicted q-values for PA and PA/OA conditions were compared to p-values for approximately 6786 metabolite pairs (Fig. 5C). For the PA-cell dataset, a p-value of 0.0488 has a corresponding q value of 0.05, which on average was associated with a correlation value (ρ) of 0.55 (Fig. 5D). This estimation of the FDR was different from the distribution seen in the PA/OA cell dataset. In PA/OA cell data, a p-value of 0.0594 has a corresponding q value of 0.05, which on average was associated with a correlation value (ρ) of 0.53 (Fig. 5D).

Comparison of the metabolite-to-metabolite network between apoptotic and steatotic cells

Metabolite-to-metabolite correlated pairs were visualized as network graphs using the Spearman ρ matrices obtained from PA and PA/OA cells (Fig. 6). For this analysis, a correlation cutoff was set at 0.55, which is greater than the minimum ρ value of 0.05 indicated by a q-value of 0.05 (Fig. 5C). The q value estimation of the FDR suggests that correlations having an absolute value greater than 0.55 are likely to be reproducible. To evaluate the significance of each element in the correlation network, we used the degree as a standard measure of centrality, and also applied a k-core analysis to generate a sequence of sub-networks that gradually reveals the globally central region of the original network. In Fig. 6, each node is characterized by shape (metabolite), size (degree of correlation) and color (“coreness”). In addition, a red or blue line corresponds to whether the relationship lies inside or outside of the coreness—k_{max}, respectively. Correlation networks in apoptotic and steatotic groups were developed using PA cells (n = 15) and PA/OA cells (n = 15), respectively (Fig. 6A and B). In PA cells, network analysis revealed a relatively higher degree of correlation among TCA cyclerelated metabolites such as citrate, glutamate and adenosine with smaller node sizes, with the glycolytic and PPP metabolites fructose-6P, ribose-5P and gluconate observed to scatter broadly among the network, generating different clusters (Fig. 6A). Notably, ceramides and other lipid molecules were observed to have smaller degrees of centrality and coreness. Thus, this network reveals weak interactions among TCA cycle, PPP and glycolysis metabolites in PA cells. By contrast, PA/OA cells show a higher degree of correlation between PPP and glycolytic metabolites, such as fructose-6P, ribose, gluconate and galactonate. In addition, TCA cycle intermediates and mono- or diacylglycerols showed relatively higher degrees of centrality and coreness in PA/OA cells, suggesting that the coordination between the TCA cycle and lipogenesis was accelerated to provide for triglyceride production in these cells (Fig. 6C).

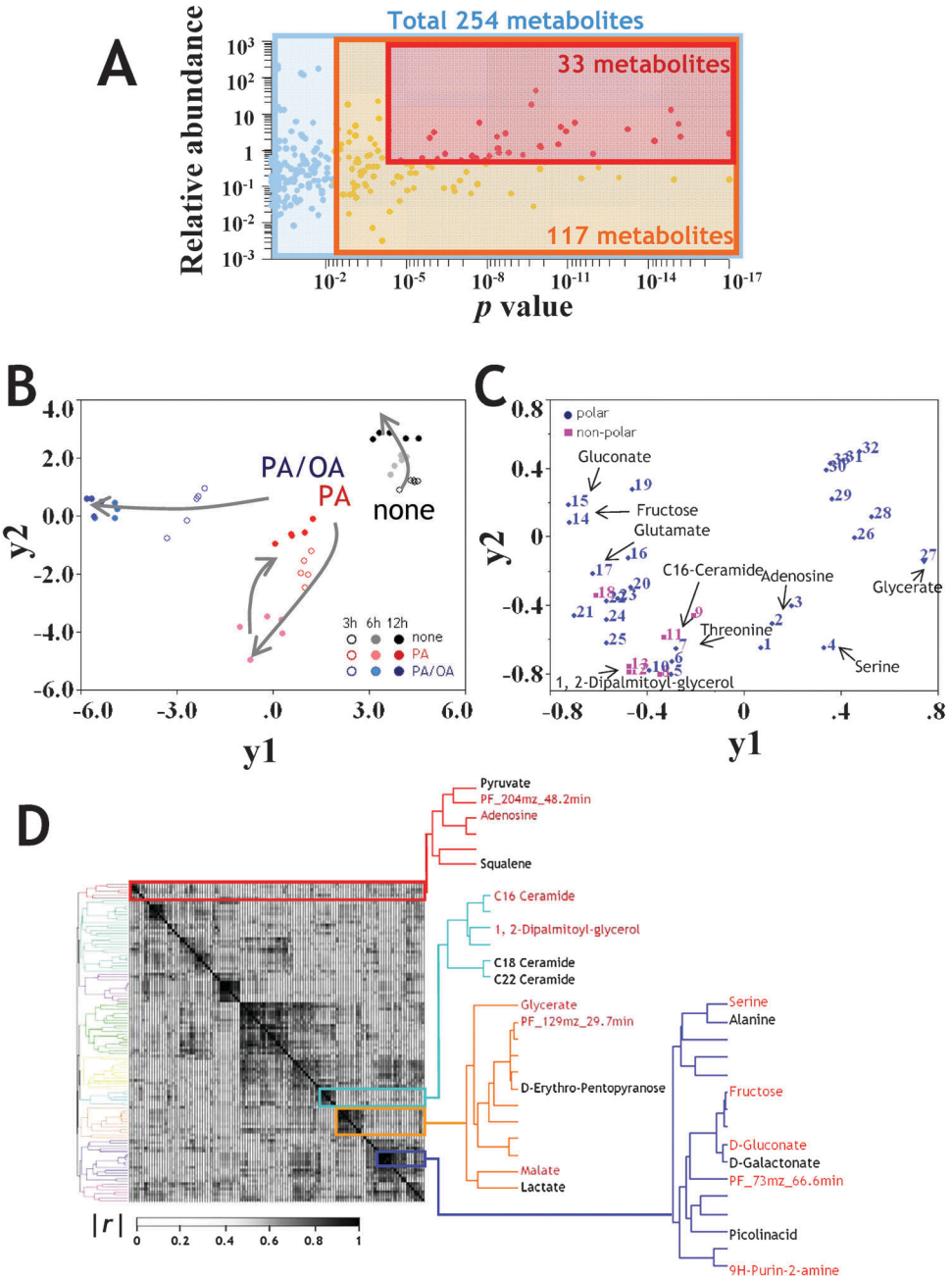

Fig. 3 Marker identification from H4IIEC3 cells developing apoptotic and steatotic phenotypes. (A) Comprehensive metabolite profiles of untreated cells, PA cells and PA/OA cells at varying incubation times (3, 6 and 12 h) were obtained using GC-MS analyses as shown in Fig. 1. In total, 254 well-conserved peaks were obtained using the SpectConnect software, and 107 metabolites were identified using the NIST05 and in-house standard libraries. Relative abundances (R.A.) against p values from the 2-way ANOVA of 254 metabolites are shown inside the blue box in panel A, with the 117 metabolites with relatively higher significance (R.A. $>$ 0.001 and $p < 0.00005$) and the 33 most abundant and significant metabolites (R.A. $>$ 0.5 and $p < 0.00005$) highlighted inside orange and red boxes, respectively. (B and C) Fisher discriminant analysis (FDA) and its loading plot. The $y1$ axis roughly corresponds to the steatotic phenotype, and the $y2$ axis represents the apoptotic phenotype. In panel B, PA and PA/OA conditions are represented by red and blue symbols, respectively, and the FDA analysis shows the time-dependent separation among the three groups. In panel C, polar and non-polar metabolites are shown as blue and pink symbols, respectively. A detailed list of marker metabolites is presented in Table 3. (D) Correlation-based clustering to explore phenotypic metabolites from the low R.A. metabolites (total 117 metabolites, orange symbols in panel A). Metabolites with red text represent highly reliable markers obtained from FDA (panel C).

Discussion

We previously used stable isotopic analyses of metabolic flux in central carbon metabolic pathways to uncover metabolic disturbances that precede the onset of apoptotic or steatotic phenotypes.[17] Our results clearly show that the activation of TCA fluxes by PA occurs concomitantly with a reduction of glycolysis and an increase in the cytosolic NAD^+/NADH

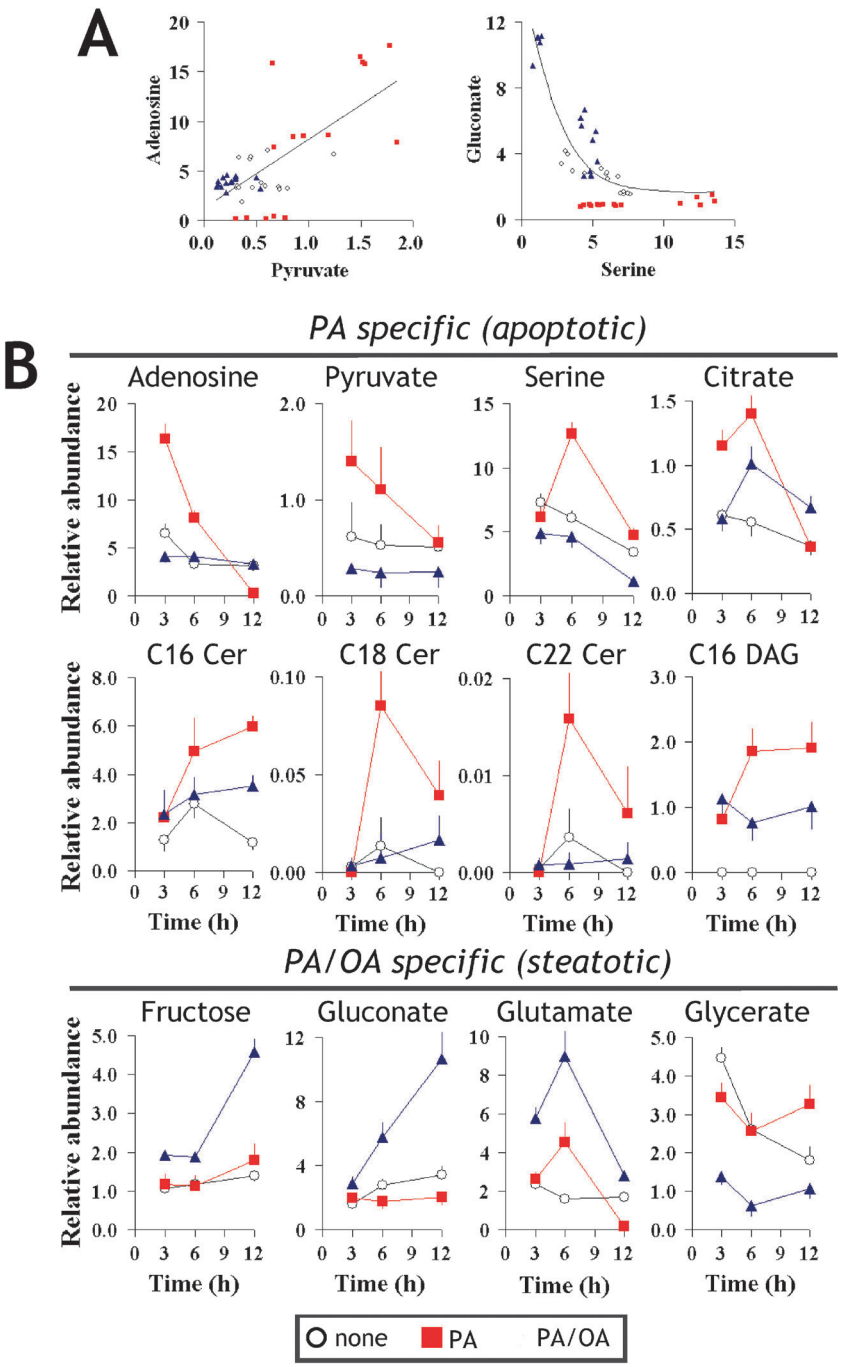

Fig. 4 Representative metabolites indicating development of both apoptotic and steatotic phenotypes. (A) Representative correlation plots of metabolites included in correlation-based clustering (panel D in Fig. 2). (B) Time-course changes of marker metabolite concentrations obtained through FDA and hierarchical clustering. Here, glycerate is shown with the PA/OA specific metabolites, although it was originally categorized as an untreated marker (group-I) in panel C. Values are expressed as mean ± S.D. (n = 5).

ratio.[17] The decoupling of glycolytic and TCA cycle fluxes was normalized after co-supplementation with OA. Also, it was found that amino acids play a modulatory role in these processes, possibly through control of central carbon fluxes. However, the mechanisms that link metabolites, metabolic flux and apoptotic or steatotic phenotypes remain unclear. In the present study, we used metabolic profiling in pre-apoptotic cells to determine what physiological events lead to ROS formation and apoptosis. Lipid profiling experiments have been used to assess levels of long-chain fatty acids, cholesterol and ceramides in PA-treated HL60 and MIN6 cells.[13,19] However, none of these studies included a comprehensive analysis of polar metabolites. Our metabolic profiling revealed perturbation of polar and non-polar metabolites in both PA and PA/OA cells. For example, we identified the condition-specific markers adenosine, TCA cycle metabolites and ceramide species in PA cells, sugar metabolites in PA/OA cells and amino acids in both PA and PA/OA cells. Adenosine was

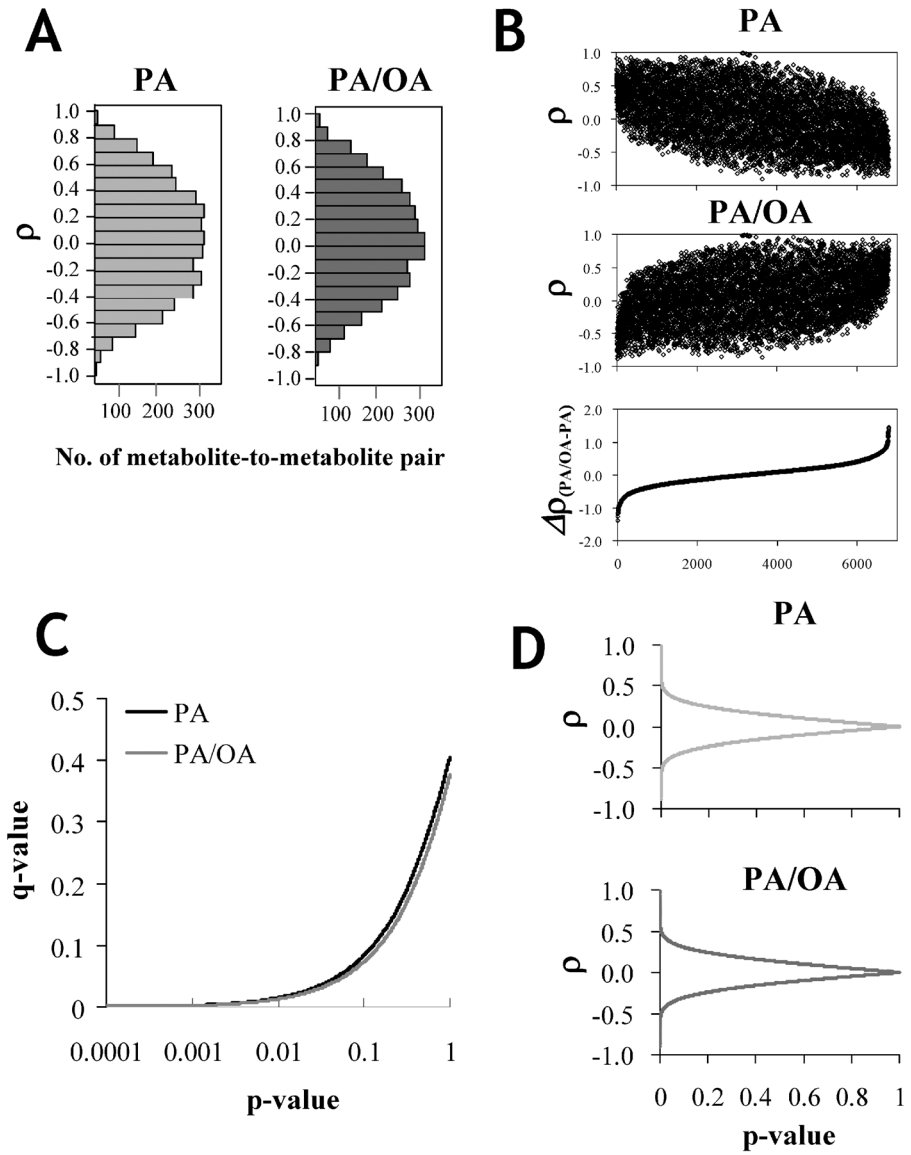

Fig. 5 Metabolite-to-metabolite correlativity in FFA-treated H4IIEC3 cells. (A) Histograms of Spearman's rank correlation (ρ) of metabolite-to-metabolite correlated pairs calculated for metabolites from PA cells (sum of 3, 6, 12 h time points, $n = 15$) and PA/OA cells (sum of 3, 6, 12 h time points, $n = 15$). In total, 6786 metabolite-to-metabolite pairs were generated from 117 metabolites described in Fig. 2A. (B) Changes in metabolite-to-metabolite correlations (ρ) after treatment with FFA. Metabolite-to-metabolite pairs are ranked in order of the change in ρ (PA/OA–PA) from negative maximum to positive maximum (bottom panel). (C) Estimation of the false discovery rate (FDR). Comparisons of q-values and p-values for the metabolite:metabolite correlates are shown for the datasets from PA-cells and PA/OA-cells; q values of 0.05 for PA-cells and PA/OA-cells are associated with p values of approximately 0.0488 and 0.0594, respectively. (D) Distribution of metabolite-to-metabolite correlations (ρ) to p-values.

strongly increased in PA cells. Recent studies have presented evidence that PA can inhibit the adenosine nucleotide translocator (ANT) in isolated mitochondria.[20,21] Inhibition of ANT has been proposed to contribute to cellular dysfunction by increasing ROS and adenosine levels by affecting the coenzyme Q redox state, mitochondrial membrane potential and cytosolic ATP concentration.[21] Furthermore, exchange of ATP and ADP *via* ANT across the mitochondrial membrane is normally cooperative with the hexokinase reaction, a first step of glycolysis.[22,23] Thus, inhibition of ANT could potentially lead to reduced glycolysis and an increased cytosolic NAD^+/NADH ratio.

Ceramide has been considered as a factor responsible for palmitate-induced apoptosis, because it also has been shown to activate apoptotic signaling. Recent studies, however, have reported that SFAs can induce apoptosis through ROS formation and endoplasmic reticulum stress without altering intracellular ceramide levels.[16] In our previous study, ceramide synthesis inhibitors had no effect on palmitate-induced ROS generation and caspase 3/7 activation, even though they completely suppressed cellular ceramide.[17] Ceramide is known to be synthesized *de novo* from palmitate and serine. We previously showed that cellular ceramide could be influenced by medium amino acid availability, but it is not involved in

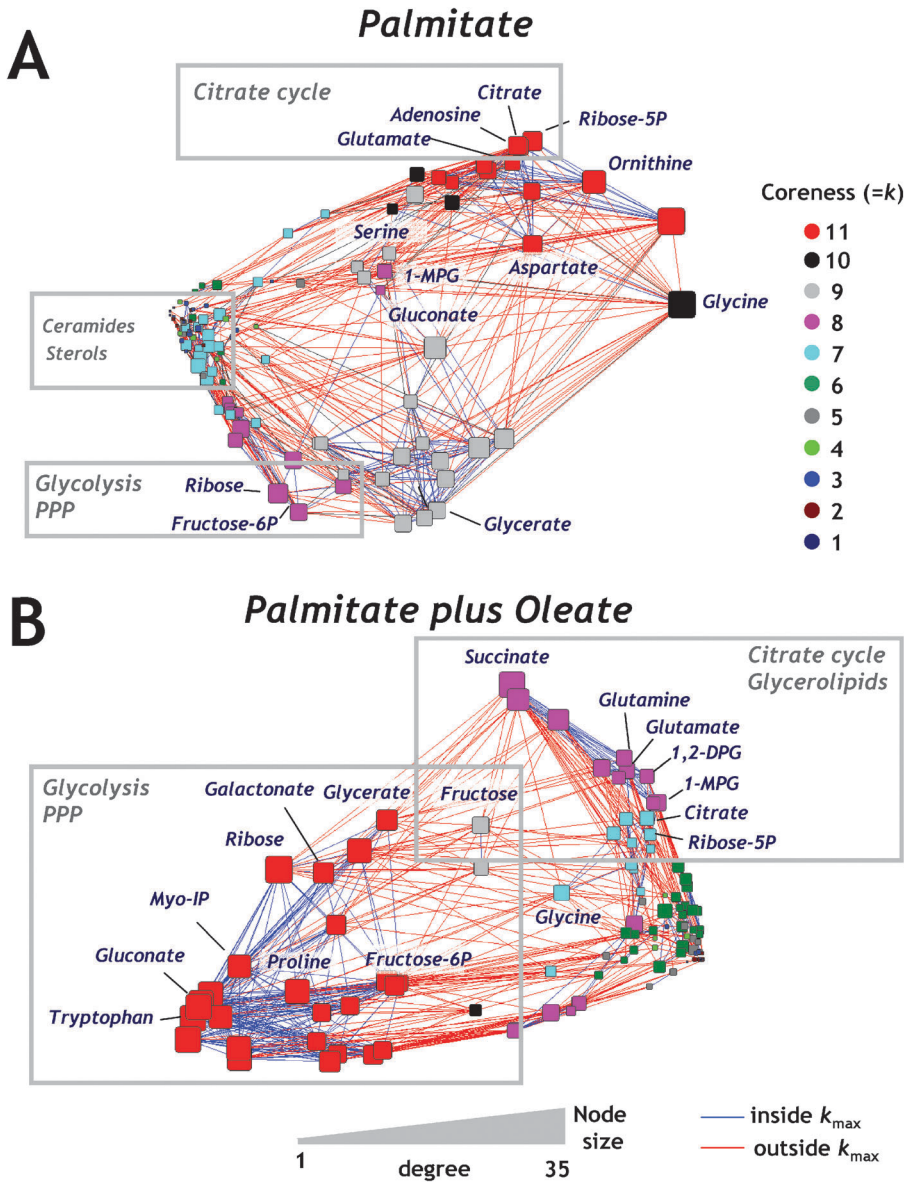

Fig. 6 Metabolite-to-metabolite correlation networks for PA cells (A) or PA/OA cells (B). Networks are generated using the Spearman ρ matrices for the 117 metabolites shown in Fig. 2A. The node shape, size, and color indicate mode (metabolite), degree, and coreness, respectively. Red or blue lines indicate whether the connected metabolites are inside or outside of the coreness—k_{max} , respectively. For this analysis, the correlation cutoff was set at 0.55, which is greater than minimum ρ of 0.53 indicated by a q-value of 0.05 (Fig. 3C). The q value estimation of the FDR suggests that correlations with an absolute value greater than 0.53 are likely to be reproducible.

both palmitate- and amino-acid-induced phenotypic changes, at least in our model.[17]

In the present study, serine and gluconate were also identified as markers of PA and PA/OA cells, respectively, and showed negative correlation with each other. Sriram *et al.* employed metabolic flux analysis using ^{13}C labeling in H4IIE cells and confirmed the presence of PPP activity in this cell line.[24] Our data cannot provide a conclusive explanation of this negative correlation, but it is likely a result of flux differences in the upper glycolytic pathway and PPP. The present network analysis illustrates weak interactions among the TCA cycle, PPP and glycolysis metabolites in PA cells. By contrast, stronger associations between PPP and glycolytic metabolites were seen in PA/OA cells. In addition, TCA cycle metabolites showed associations with glycerolipid intermediates only in PA/OA cells, indicating that the increased TG synthesis caused by OA co-treatment was accompanied by modulation of flux through the TCA cycle. Thus, these data suggest that changes in PPP flux might be also related to the decoupling of flux through the glycolytic pathway and TCA cycle *via* the modulation of PA concentration in cells developing an apoptotic phenotype.

Conclusion

In the present study, we applied GC-MS-based, comprehensive metabolic profiling to track metabolomic changes in cells

developing lipoapoptotic and steatotic phenotypes, and we successfully identified phenotype-specific changes. We believe that our methods can be used as powerful tools for the discovery of metabolic profiles in various mammalian cell models. Further studies will be needed to determine the significance of all identified metabolites in these lipoapoptotic and steatotic phenotypes.

Experimental procedures

Materials

Free amino acids were purchased from Sigma (St. Louis, MO, USA). Fatty-acid-free bovine serum albumin (BSA) was purchased from JRH Biosciences (Lenexa, KS, USA). Amino-acid-free Dulbecco's modified Eagle's medium (DMEM) was a gift from Ajinomoto (Tokyo, Japan). All silylation reagents used in this study were purchased from Pierce (Rockford, IL, USA).

Cell culture

H4IIEC3 cells (American Type Culture Collection, Manassas, VA, USA) were cultured in DMEM supplemented with 10% fetal bovine serum, 50 units per ml penicillin and 50 units per ml streptomycin sulfate. Medium was changed to a customized medium containing 25 mM glucose, 2.15 mM amino acids, amino-acid-free DMEM, 20 mM HEPES and 0.5% serum replacement 3 with or without FFA–BSA complex. Based on our previous study,[17] the amino acid composition was designed to resemble rat plasma amino acids (Table 1). Metabolites in the intracellular compartment were analyzed by GC-MS at 3, 6 and 12 h.

Table 1 Comparison of physiological and medium amino acids. Rat plasma amino acids are cited from our previous study[17]

	Plasma	Culture medium	
Amino acid	Rat	DMEM	This study
Histidine	45–90	200	50
Isoleucine	30–115	800	50
Leucine	40–195	800	100
Lysine	80–285	800	200
Methionine	30–100	200	50
Phenylalanine	34–85	400	50
Threonine	55–270	800	100
Tryptophan	30–105	100	50
Valine	55–235	800	150
Alanine	220–460	400	250
Arginine	36–143	400	80
Asparagine	35–58	0	50
Asparatate	38–90	0	20
Cystine	10–56	200	50
Glutamate	42–94	0	50
Glutamine	375–700	4000	450
Glycine	105–460	400	150
Proline	100–200	0	100
Serine	110–210	400	100
Tyrosine	30–100	400	50
Essential/non-essential	0.30–0.66	0.79	0.59
Total	1875–3500	11 100	2150

ROS measurement

Cellular ROS generation was measured using H_2DCFDA (Invitrogen, Carlsbad, CA, USA) as described previously.[25] H_2DCFDA is a non-polar compound that readily diffuses into cells, where it is hydrolyzed by intracellular esterases to the nonfluorescent molecule dichlorodihydrofluorescein, which remains trapped within the cells. In the presence of a proper oxidant, dichlorodihydrofluorescein is oxidized to the highly fluorescent 2,7-dichlorofluorescein. Cells treated with various fatty acids or amino acids were incubated with 10 μM H_2DCFDA for 30 min at 37 °C in the dark, then resuspended with Hanks balanced salt solution (HBSS). The fluorescence intensity was measured at an excitation/emission wavelength of 490/530 nm using a FusionTM universal microplate analyzer (PerkinElmer, Shelton, CT, USA).

Nile red staining

Cells were cultured in 96-well plates with or without FFA. After a 24 h incubation, cells were stained with Nile red using AdipoRed reagent (Cambrex, East Rutherford, NJ, USA). Intracellular lipid accumulation was observed using a fluorescence microscope and quantified using a microplate analyzer at an excitation/emission wavelength of 485/590 nm.

Cell viability

Cultured cells in 96-well plates were washed twice with PBS and then incubated with serum-free DMEM for 4 h at 37 °C. Cellular metabolic capacity was measured based on reduction of resazurin using the CellTiter-Blue® cell viability assay (Promega, Madison, WI, USA).

Metabolite extraction

We employed a biphasic extraction protocol, with non-polar metabolites partitioning into a chloroform phase and polar metabolites partitioning into a methanol/water phase. Cells cultured in 100 mm dishes were washed twice with ice-cold

Table 2 FFA-induced apoptosis and steatosis in H4IIEC3 cells under physiological amino acids

	Cellular lipids (Nile red fluorescence)		ROS (DCF fluorescence)		Cell viability (Resazurin reduction)	
Untreated	3837 ± 143	(100)	4292 ± 584	(100)	1.0 ± 0.073	(100)
400 μM PA	17 064 ± 980*	(445)	9732 ± 154*	(227)	0.44 ± 0.041*	(44)
400 μM PA + 10 μM OA	19 384 ± 1054*	(505)	6752 ± 1334*	(157)	0.54 ± 0.070*	(54)
400 μM PA + 50 μM OA	30 718 ± 920*	(801)	4934 ± 621	(115)	0.96 ± 0.063	(96)
400 μM PA + 200 μM OA	35 678 ± 1444*	(930)	4201 ± 244	(98)	0.99 ± 0.045	(99)
400 μM OA	20 167 ± 1497*	(526)	2460 ± 1056*	(57)	0.95 ± 0.049	(95)

Values are expressed as mean ± SEM ($n = 3$). *$p < 0.05$ for the comparison with untreated cells. Values in parentheses are percent control.

Table 3 Phenotypic metabolites in FFA treated H4IIEC3 cells

No.	Loading ($y2/y1$)[a]	Metabolite	Fr.[b]	Ion[c]/m/z	RT[d]/min	Description from best library hit	Probability (%)
1	−9.16	Unknown	PF	204	48.2	No library fit	<20
2	−4.28	Adenosine	PF	230	67.5	Adenosine-tetrakis (trimethylsilyl)	98.4
3	2.69	Citrate	PF	273	43.9	Citric acid, tetrakis (trimethylsilyl)	74.9
4	2.47	Aspartate	PF	232	29.1	L-Aspartic acid, *N*-(trimethylsilyl)-, bis(trimethylsilyl) ester	91.5
5	2.33	Threonine	PF	218	21.7	*N,O,O*-Tris-(trimethylsilyl)-L-threonine	96.8
6	2.32	1-Monopalmitoyl-glycerol	NF	371	22.3	1-Monopalmitin trimethylsilyl ether	94.3
7	2.22	2-Monopalmitoyl-glycerol	NF	218	21.9	2-Monopalmitin trimethylsilyl ether	88.0
8	−2.03	Malate	PF	233	27.7	Tris(trimethylsilyl) malic acid	78.5
9	2.00	Unknown	PF	171	26.5	No library fit	<20
10	−1.96	Serine	PF	204	20.8	*N,O,O′*-Tris-(trimethylsilyl)-serine	79.0
11	1.79	C16 Ceramide	NF	370	51.1	In-house library hit	n/a
12	1.68	Unknown	NF	73	11.4	No library fit	<20
13	1.61	1,2-Dipalmitoyl-glycerol	NF	145	53.0	2-(Palmitoyloxy)-1-([(trimethylsilyl)oxy]methyl)ethyl palmitate	87.8
14	1.20	Glycine	PF	174	17.9	Glycine, *N,N*-bis(trimethylsilyl)-, trimethylsilyl ester	90.2
15	1.15	Unknown	PF	73	55.9	No library fit	<20
16	1.09	Myo-inositol-phosphate	PF	318	66.8	D-Myo-inositol,1,2,4,5,6-pentakis-*O*-(trimethylsilyl)-, 2,3-bis[(trimethylsilyl)oxy]propyl trimethylsilyl phosphate	97.0
17	1.09	Unknown	PF	147	55.0	No library fit	<20
18	1.05	Unknown	PF	217	56.7	No library fit	<20
19	0.86	Unknown	PF	113	20.8	No library fit	<20
20	0.70	Proline	PF	142	18.9	*N,O*-Bis-(trimethylsilyl)-proline	93.6
21	0.66	Glutamine	PF	156	33.4	In-house library hit	n/a
22	0.66	*N*-Acetyl-glutamate	PF	174	32.5	Bis(trimethylsilyl) 2-(acetylamino)pentanedioate	52.6
23	0.64	Unknown	PF	446	63.9	No library fit	<20
24	−0.62	Unknown	PF	73	66.6	No library fit	<20
25	0.61	Unknown	PF	129	29.7	No library fit	<20
26	0.56	Desmosterol	NF	129	36.9	Cholesta-5,24-diene, 3β-(trimethylsiloxy)-	95.5
27	0.34	Glutamate	PF	246	34.0	L-Glutamic acid, *N*-(trimethylsilyl)-, bis(trimethylsilyl) ester	90.4
28	0.26	9H-Purin-2-amine	PF	324	69.5	9H-Purin-2-amine, *N*-(trimethylsilyl)-6-[(trimethylsilyl)oxy]-9-[2,3,5-tris-*O*-(trimethylsilyl)-β-D-ribofuranosyl]-	87.7
29	−0.26	D-Gluconate	PF	333	46.0	D-Gluconic acid, 2,3,4,5,6-pentakis-*O*-(trimethylsilyl)-, trimethylsilyl ester	76.2
30	0.22	Unknown	PF	305	49.9	No library fit	<20
31	−0.19	Glycerate	PF	292	19.7	Glyceric acid, tris(trimethylsilyl)	95.9
32	−0.12	Unknown	PF	247	34.5	No library fit	<20
33	−0.01		PF	307	42.9	D-Fructose, 1,3,4,5,6-pentakis-*O*-(trimethylsilyl)-, *O*-methyloxime	88.6

[a] $y2/y1$ values of each metabolite in Fig. 3C. [b] Fraction (Fr.) in extraction process: PF, polar fraction; NP, non-polar fraction. [c] Specific ion of each marker metabolite. [d] Retention time (RT). n/a, Not applicable.

PBS and immediately quenched with 1 ml pre-cooled methanol (−80 °C). Cells were collected in glass tubes with a cell scraper (BD Biosciences, San Jose, CA, USA). Cells were resuspended with 1 ml ice-cold water, and the remaining cells were combined in the same tubes. For determination of protein concentration, 20 μl of cell suspension was taken from the sample tubes and stored at −80 °C.

To prepare samples for GC-MS analysis, 15.8 nmol trihepta-decanoin, 4.96 nmol pentadecanoate, 2.94 nmol 5α-cholestane and 4.2 nmol *N*-pentadecanoyl-sphingosine (C15 ceramide) in 30 μl chloroform (non-polar internal standards) and also 9.9 nmol ribitol in 30 μl methanol (polar internal standards) were added. After addition of 1 ml chloroform, samples were shaken for 30 min at room temperature and then 3 ml chloroform and 2 ml water were added. Vortexed samples were centrifuged at 4000*g* for 30 min at room temperature. Two 2 ml extracts from the methanol/water phase or non-polar samples from the chloroform phase were separately collected in new tubes and then evaporated to dryness. All samples were stored at −80 °C until analysis. The protein content for each sample was quantified using a BCA assay kit (Pierce, Rockford, IL, USA).

Polar metabolite analysis

Derivatization of polar metabolites was performed according to previous studies.[17,26] One of each pair of dried samples was dissolved in 30 μl of methoxyamine hydrochloride (20 mg per ml in pyridine). Sample solutions were sonicated for 15 min at room temperature and incubated for 120 min at 37 °C. After incubation, 70 μl MBTSTFA + 1% TBDMCS was added and the solutions were further incubated overnight at room temperature.

Gas chromatography-mass spectrometry (GC-MS) analysis was performed using an Agilent 6890N GC equipped with a 30 M DB-35ms capillary column connected to an Agilent 5975B MS operating under ionization by electron impact (EI) at 70 eV. An injection volume of 1 μl was introduced in splitless mode at an injection temperature of 270 °C. The temperature of the MS source and quadrupole were held at 230 °C and 150 °C, respectively. The detector was set to scan over the mass range 50–550 m/z. The GC temperature program was optimized to follow a large number of metabolites simultaneously: 5 min at 90 °C, 60 min ramp to 280 °C and held for 5 min at 280 °C (total 70 min per run).

Non-polar metabolite analysis

For non-polar metabolite analysis, dried non-polar samples were dissolved in 1.55 ml of isooctane : methanol : ethyl acetate (20 : 10 : 1). To remove triglycerides, samples were applied to a silica gel-packed Poly-Prep column (BIO-RAD, Hercules, CA, USA) as previously described.[27,28] Eluted free lipid fractions were evaporated to dryness. For ceramide analysis, samples were re-dissolved in 250 μl of phosphate buffer (0.1 M, pH 7.0) containing 0.1 U sphingomyelinase and 1 mM $MgCl_2$. Free lipid fractions were extracted three times in 500 μl isooctane: ethyl acetate (3 : 1) and then evaporated to dryness. Samples were dissolved in 150 μl BSTFA + 1% TMCS: acetonitrile (4 : 1) and then incubated overnight at room temperature. GC-MS analysis of free lipids was performed with the following parameter settings. The temperatures of the injection port, MS source and quadrupole were set at 310 °C, 230 °C and 150 °C, respectively. The GC temperature program was set as follows: 3 min at 130 °C, 4 min ramp to 190 °C, 3 min at 190 °C, 12.3 min ramp to 264 °C, 5 min at 264 °C, 5.75 min ramp to 287 °C, 8 min at 287 °C, 4.6 min ramp to 310 °C, 3 min at 310 °C, 4.7 min ramp to 325 °C, and 16.6 min at 325 °C (total 70 min per run).

GC-MS data analysis

All GC-MS data were analyzed according to the method of Styczynski *et al.*[29] Briefly, mass spectra were processed using AMDIS software (http://chemdata.nist.gov/mass-spc/amdis/; National Institute of Standards and Technology). The resulting ELU files were further analyzed by the SpectConnect software (http://spectconnect.mit.edu/), developed by our laboratory, to identify well-conserved peaks among multiple GC-MS chromatograms. SpectConnect can automatically catalog and track otherwise unidentifiable conserved metabolite peaks across sample replicates and different sample condition groups without use of reference spectra. SpectConnect compares every spectrum in each sample to the spectra in every other sample. By doing so, it is capable of determining which components are conserved across replicate samples. SpectConnect also determines which of these components differentiate one sample condition (*e.g.*, time or treatment) from another, whether by changes in concentrations or merely by their presence/absence. The only requirement of the experimental measurements is that each sample condition must have replicates. In a sense, SpectConnect relies on an increase in signal relative to noise that is created by this requirement of replicates.[29] In the present study, all experiments were examined by biological replications in a group of samples ($n = 5$). Metabolite identification of EI-MS peaks was performed using in-house standard libraries along with the NIST05 MS library described in previous paper.[30] Two-dimensional clustering of metabolite correlativity was performed using JMP (SAS Institute Inc., Cary, NC, USA).

Correlation-based metabolite-to-gene network analysis

Correlation networks were constructed in accord with the previously reported method.[31] To uncover possible interactions between two entities i (=metabolite X) and j (=metabolite Y), the Pearson or Spearman's rank correlation coefficient ρ_{ij} was calculated for each pair within the obtained dataset. The significance of each pair of metabolite and transcript correlations was assessed using the FDR by estimating a q-value for each correlated pair[32] The q-value measures the predicted FDR associated with a significant test when multiple hypotheses are tested, *i.e.*, a q-value of 0.05 implies that for every 100 significant correlates, five false correlated pairs are expected. A comparison of multiple false discovery estimations on several -omics datasets suggests that the q-value method has a high apparent power and strong control of the FDR. By eliminating the associations with lower $|\rho_{ij}|$ pairs ($n = 15$–30), we selected only the networks that contained highly significant correlated entities.

To measure centrality in metabolite–metabolite correlation datasets or a projected bipartite network, several standard measures of centrality can be used, such as degree, closeness, betweenness and eigenvector centrality.[33] In the present study, we used degree as a standard measure of centrality, where the degree of centrality of a node is defined as the number of edges incident upon that node. In the case of the correlation of a metabolite and transcript, this means that the degree of a metabolite is the number of transcripts that relate to the metabolite, and the degree of a transcript is the number of metabolites that relate with the other metabolites. Thus, degree has a clear and simple interpretation in the correlation network. In addition, we introduced the k-core decomposition as an additional dimension to visualize complex networks.[34] This decomposition, based on a recursive pruning of the least connected vertices, allows disentanglement of the hierarchical structure of networks by progressively focusing on their central cores. The k-core decomposition consists of k-cores that identify particular subsets; each one was obtained by recursively removing all vertices having a degree smaller than k until the degree of all the remaining vertices became greater than or equal to k ($0, 1, 2, \ldots k_{max}$). Larger values of "coreness" simply correspond to vertices with larger degrees and more central positions in the given network.[35]

Statistics

Statistical significance among the groups was determined by Tukey's honestly significant difference test after ANOVA for multiple comparisons. All correlation analyses were performed using JMP. Fisher discriminant analysis (FDA) was performed using our lab's original software BioSystAnse 1.07. The false discovery rate (FDR) for each metabolite-to-gene correlate pair was estimated as a q-value using software created by Alan Dabney and John Storey.[36] For generation of metabolite-to-gene network images, UCINET version 6.34 (Analytic Technologies Inc., Harvard, MA) was used.

This work was supported by NIH DK075850 and NIH ES013925. J.D.Y. was supported by NIH grant F32 DK072856.

Abbreviations

1,2-DPG	1,2-dipalmitoyl-glycerol
Fructose-6P	fructose-6-phosphate
1-MPG	1-monopalmitoyl-glycerol
MUFA	monounsaturated fatty acid
Myo-IP	Myo-inositol-phosphate
Ribose-5P	ribose-5-phosphate

References

1 M. Cuperlovic-Culf, D. A. Barnett, A. S. Culf and I. Chute, *Drug Discovery Today*, 2010, **15**, 610–621.
2 M. Heinemann and R. Zenobi, *Curr. Opin. Biotechnol.*, 2010, **22**, 1–6.
3 S. Tiziani, A. Lodi, F. L. Khanim, M. R. Viant, C. M. Bunce and U. L. Gunther, *PLoS One*, 2009, **4**, e4251.
4 Y. Si, H. Shi and K. Lee, *PLoS One*, 2009, **4**, e7000.
5 S. Lin, N. Liu, Z. Yang, W. Song, P. Wang, H. Chen, M. Lucio, P. Schmitt-Kopplin, G. Chen and Z. Cai, *Talanta*, 2010, **83**, 262–268.
6 G. Catchpole, A. Platzer, C. Weikert, C. Kempkensteffen, M. Johannsen, H. Krause, K. Jung, K. Miller, L. Willmitzer, J. Selbig and S. Weikert, *J. Cell. Mol. Med.*, 2009.
7 A. Ramanathan, C. Wang and S. L. Schreiber, *Proc. Natl. Acad. Sci. U. S. A.*, 2005, **102**, 5992–5997.
8 O. Yanes, J. Clark, D. M. Wong, G. J. Patti, A. Sanchez-Ruiz, H. P. Benton, S. A. Trauger, C. Desponts, S. Ding and G. Siuzdak, *Nat. Chem. Biol.*, 2010, **6**, 411–417.
9 L. L. Listenberger, D. S. Ory and J. E. Schaffer, *J. Biol. Chem.*, 2001, **276**, 14890–14895.
10 A. Wieckowska, A. J. McCullough and A. E. Feldstein, *Hepatology*, 2007, **46**, 582–589.
11 L. L. Listenberger, X. Han, S. E. Lewis, S. Cases, R. V. Farese, Jr., D. S. Ory and J. E. Schaffer, *Proc. Natl. Acad. Sci. U. S. A.*, 2003, **100**, 3077–3082.
12 I. C. Okere, M. P. Chandler, T. A. McElfresh, J. H. Rennison, V. Sharov, H. N. Sabbah, K. Y. Tserng, B. D. Hoit, P. Ernsberger, M. E. Young and W. C. Stanley, *Am. J. Physiol.: Heart Circ. Physiol.*, 2006, **291**, H38–44.
13 A. K. Busch, E. Gurisik, D. V. Cordery, M. Sudlow, G. S. Denyer, D. R. Laybutt, W. E. Hughes and T. J. Biden, *Diabetes*, 2005, **54**, 2917–2924.
14 F. J. Barreyro, S. Kobayashi, S. F. Bronk, N. W. Werneburg, H. Malhi and G. J. Gores, *J. Biol. Chem.*, 2007, **282**, 27141–27154.
15 H. Malhi, S. F. Bronk, N. W. Werneburg and G. J. Gores, *J. Biol. Chem.*, 2006, **281**, 12093–12101.
16 R. H. Unger and Y. T. Zhou, *Diabetes*, 2001, **50**(Suppl 1), S118–121.
17 Y. Noguchi, J. D. Young, J. O. Aleman, M. E. Hansen, J. K. Kelleher and G. Stephanopoulos, *J. Biol. Chem.*, 2009, **284**, 33425–33436.
18 W. Guo, S. Wong, W. Xie, T. Lei and Z. Luo, *Am. J. Physiol.: Endocrinol. Metab.*, 2007, **293**, E576–586.
19 K. Y. Tserng and R. L. Griffin, *Biochem. J.*, 2004, **380**, 715–722.
20 J. Ciapaite, S. J. Bakker, M. Diamant, G. van Eikenhorst, R. J. Heine, H. V. Westerhoff and K. Krab, *FEBS J.*, 2006, **273**, 5288–5302.
21 J. Ciapaite, G. van Eikenhorst and K. Krab, *Mol. Biol. Rep.*, 2002, **29**, 13–16.
22 A. Chevrollier, D. Loiseau, B. Chabi, G. Renier, O. Douay, Y. Malthiery and G. Stepien, *J. Bioenerg. Biomembr.*, 2005, **37**, 307–316.
23 J. G. Pastorino, N. Shulga and J. B. Hoek, *J. Biol. Chem.*, 2002, **277**, 7610–7618.
24 G. Sriram, L. Rahib, J. S. He, A. E. Campos, L. S. Parr, J. C. Liao and K. M. Dipple, *Mol. Genet. Metab.*, 2008, **93**, 145–159.
25 G. Sudhandiran and C. Shaha, *J. Biol. Chem.*, 2003, **278**, 25120–25132.
26 Y. Noguchi, N. Nishikata, N. Shikata, Y. Kimura, J. O. Aleman, J. D. Young, N. Koyama, J. K. Kelleher, M. Takahashi and G. Stephanopoulos, *PLoS One*, 2010, **5**, e12057.
27 K. Y. Tserng and R. Griffin, *Anal. Biochem.*, 2003, **323**, 84–93.
28 C. Vieu, F. Terce, F. Chevy, C. Rolland, R. Barbaras, H. Chap, C. Wolf, B. Perret and X. Collet, *J. Lipid Res.*, 2002, **43**, 510–522.
29 M. P. Styczynski, J. F. Moxley, L. V. Tong, J. L. Walther, K. L. Jensen and G. N. Stephanopoulos, *Anal. Chem.*, 2007, **79**, 966–973.
30 Y. Tikunov, A. Lommen, C. H. de Vos, H. A. Verhoeven, R. J. Bino, R. D. Hall and A. G. Bovy, *Plant Physiol.*, 2005, **139**, 1125–1137.
31 Y. Noguchi, N. Shikata, Y. Furuhata, T. Kimura and M. Takahashi, *Physiol. Genomics*, 2008, **34**, 315–326.
32 B. Z. Ring, S. Chang, L. W. Ring, R. S. Seitz and D. T. Ross, *BMC Genomics*, 2008, **9**, 74.
33 S. P. Borgatti and M. G. Everett, *Soc. Networks*, 1997, **19**, 243–269.
34 J. I. Alvarez-Hamelin, L. Dall'Asta, A. Barrat and A. Vespignani, *Adv. Neural Inf. Process. Syst.*, 2006, **18**, 41 http://arxiv.org/abs/cs.ni/0504107.
35 S. Wachi, K. Yoneda and R. Wu, *Bioinformatics*, 2005, **21**, 4205–4208.
36 Q-Value, [http://faculty.washington.edu/jstorey/qvalue/].